Tribology Letters (2023) 71:15
https://doi.org/10.1007/s11249-022-01675-3

ORIGINAL PAPER

Research on the Dynamic Behaviors in the Sliding Friction of Silicone

Yunlong Gao[1] · Yongjuan Wang[1]

Received: 22 May 2022 / Accepted: 4 November 2022 / Published online: 19 December 2022

Abstract
With the promotion of soft viscoelastic materials in the field of flexible bionic robots, the behavior of sliding friction between soft viscoelastic materials and rigid materials such as metals has attracted great attention. In this study, the research object was silicone, and a research method combining a dynamic force testing technique and a non-contact optical testing technique for deformation and strain was proposed to study the frictional behavior of silicone and the effect of the tooth structure surface on the sliding friction. We analyzed the temporal changes in the friction force for different loads, the dynamic characteristics of large deformation and micro-strain on the front side (define the contact surface as the bottom surface) of the silicone. The results showed that within a certain range, the sliding friction coefficient of the silicone increased monotonically with increasing load, and there were stick-slip and deformation waves during the relative motion. The larger the load was, the faster the deformation wave propagated, and the tooth structure surface had sliding friction anisotropy.

Keywords Sliding friction of silicone · Stick-slip · Deformation wave · Non-contact stress-strain test method

1 Introduction

With the booming development of bionic technology, the combination structure of a rigid body skeleton and a soft viscoelastic body skin has become widely used in crawling bionic robots. Owing to the unique movement gait of crawling bionic robots, the dynamic characteristics of sliding friction between soft viscoelastic materials and rigid materials are worth investigating [1, 2]. For example, the meandering gait of a snake robot relies mainly on the normal friction of the skin surface in contact with the ground being greater than the tangential friction [3, 4]. The creeping gait of a silkworm-like robot is achieved with the difference in the friction forces on the skin surface in the forward and backward motion directions [5], and the sloping climbing gait of a lizard-like robot relies on the adhesion of the foot suction cups to a sloping surface [6].

The sliding friction behavior of the materials for soft viscoelastic bodies has unique properties compared to conventional rigid materials. The macroscopic friction behavior of the surfaces of soft viscoelastic materials during their motion relative to rigid materials is special, including Schallamac waves [7–11], stick-slip [12, 13], and other behaviors. For the study of sliding friction behavior, optical testing techniques are very applicable. In reference [14], the effect of the velocity on the sliding friction behavior of a smooth glass ball and an elastomer was studied with the analysis of the transmissive intensity of Schallamac waves with stick-slip. With the emergence and development of DIC (Digital Image Correlation) technology, this technology has been gradually applied to micromechanical studies. For example, in reference [15], DIC was used to study the micromechanics of a multi-contact interface formed between a rough elastomer and a smooth glass surface, and to locally probe the spatial distribution of the tangential displacement and the associated shear stress averaged over the micrometric thickness of a heterogeneous multi-contact interface. In reference [16], the dynamic crack extension behavior of polymer beams during impact loading was studied in combination with a rotating mirror-type high-speed digital camera. In reference [17], the sliding motion of a rubber specimen on

Yunlong Gao and Yongjuan Wang have contributed equally to this work.

✉ Yongjuan Wang
13951643935@139.com

Yunlong Gao
m18351897802@163.com

[1] School of Mechanical Engineering, Nanjing University of Science and Technology, No. 200, Xiaolingwei, Nanjing 210094, Jiangsu, China

a glass plate was studied and the local sliding velocity field in the contact area was obtained based on the digital image correlation method.

Silicone is widely used as a bionic material because of its good toughness, good tear resistance, and fast reshaping. However, it is difficult to use the contact test method (For example, the measurement method using strain gauges.) because silicone experiences large deformation in sliding friction. Therefore, this study proposes a research method combining a dynamic force testing technique and a non-contact optical testing technique for deformation and strain for the study of the dynamic characteristics of sliding friction between silicone and metal materials. First, the processes of test specimen preparation and test system construction are described. The purpose of the test is to obtain the mechanical dynamic characteristics of the sliding friction, the macroscopic friction behavior, and the effects of the load and the tooth surface structure on the sliding friction coefficient, and to design the test program. Next, the processes and the analysis of the friction force test data and deformation-strain test data are described. Finally, the mechanisms of the occurrences of macroscopic frictional behaviors such as stick-slip and deformation waves are studied, and conclusions are drawn accordingly.

2 Materials and Methods

This study proposed an experimental research method for determining the dynamic characteristics of silicone in sliding friction. The sliding friction coefficient was analyzed by combining the dynamic measurement method of friction with the classical friction law, and the deformation and the strain were measured with the DIC optical non-contact measurement technique. The silicone friction characteristics were analyzed based on the experimental measurement results.

2.1 Friction Force Measurement

The silicone for the test in this research was made with mold injection with two types of contact planes, smooth and toothed. Its structure and dimensions are shown in Fig. 1. Its production process was as follows. First, the mold was made with 3D printing technology. Then the curing agent was mixed with the substrate in a ratio of 1:1 and poured into the mold, and the air bubbles on the surface of the mixture were purged. Finally, the material was placed at a room temperature of 25 °C for 10 h until solidification.

The friction test method of the silicone material is shown in Fig. 2. The silicone was placed on a metal mobile module with a surface roughness of Ra0.4, a load block was added above, and the force sensor was connected to the left end of the silicone with a rope. The mobile module was driven to the right so that relative movement of the silicone and the mobile module tightened the rope. The value measured by the sensor was the friction force generated between the silicone and the mobile module.

The contact deformation and strain test method have uncontrollable environmental factors interfering with the frictional motion process. Therefore, in this research, a deformation and strain testing method based on the DIC optical non-contact measurement technique was applied, as shown in Fig. 3. First, the images of the silicone

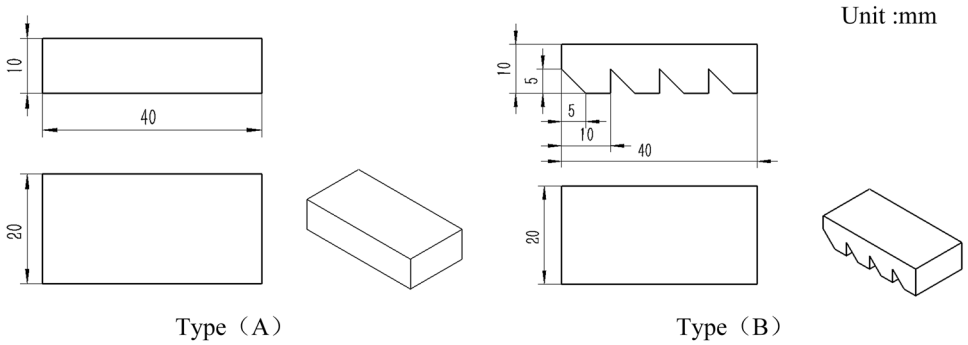

Fig. 1 Type(A) is the smooth surface rectangular silicone, Type(B) is the tooth structure surface silicone

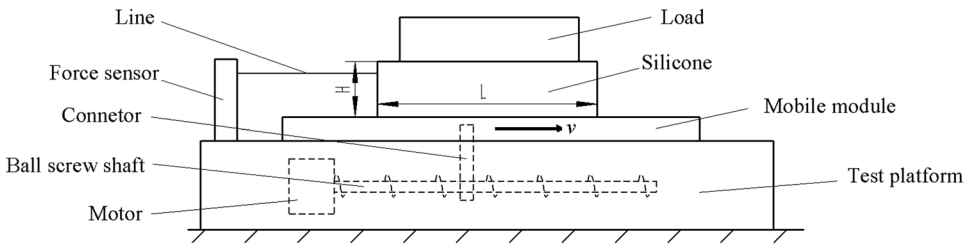

Fig. 2 Friction force measurement method

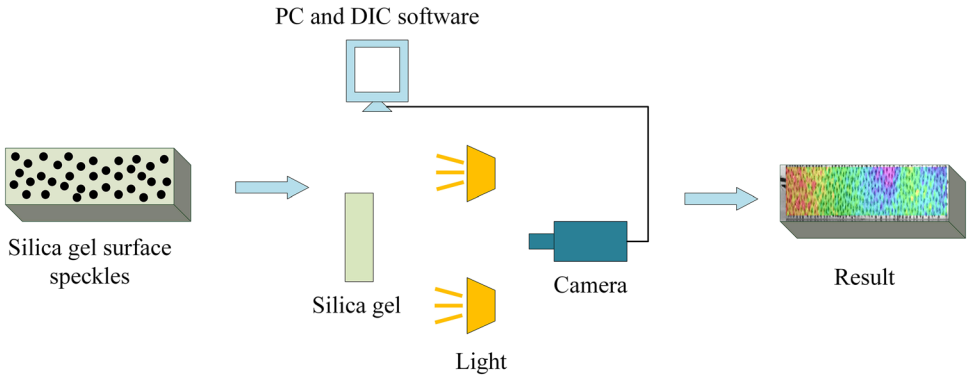

Fig. 3 DIC optical non-contact deformation and strain measurement method

rubbing process were captured by cameras. Then the randomly distributed speckles features of the silicone surface in different images were compared. The speckles were randomly distributed on the front side (define the contact surface as the bottom surface) of the silicone as shown in Fig. 2, The diameter of the speckles was random in the range of 1–2mm, The randomness of the size and distribution of the speckles was beneficial to the accuracy of the DIC analysis results. Due to the poor adhesion of the silicone surface, the traditional method of preparing the speckles using the transfer technique was not suitable, and after trying and comparing various methods, it was decided that the best results were obtained by hand painting with ink. Next, the silicone surface deformation information was calculated based on digital image correlation algorithms. Finally, the data for the deformation and strain of the silicone surface were obtained.

3 Results

In this research, the experimental scheme was designed based on the test method described in Sect. 2 . The relative sliding speed between the platform and the silicone was 100 mm/min. The weight of the silicone is 32 g. Excluding the weight of the silicone itself, the additional normal load was divided into four levels of 0 N, 0.01 N, 0.02 N, and 0.03 N. Silicone on the surface of the tooth structure did not add an additional load. Five independent tests were replicated for each load to ensure the reliability of the results. During a sliding motion, the temporal changes in the friction force were obtained with a force sensor and a data logger at a sampling rate of 25 Hz. The temporal changes in the randomly distributed speckles features of the silicone surface were captured by the high-speed camera at frame rates in the range of 70 fps, and the data were processed to obtain the subsequent results.

3.1 Dynamic Characteristics of Silicone in Sliding Friction with Different Normal Loads

The average displacement method was used to remove the effect of rigid displacement during the displacement field data processing. The average displacement method calculated the average movement of each image and then removed the average movement to obtain a displacement-deformed image without rotation. In Fig. 4a, it can be seen that the sliding friction coefficients under different normal loads have obvious differences, and the coefficients increase with the increase of the load. The standard deviation of the five sets of test data with the same load is less than 0.08. The monotonically increasing relationship between the mean value of the sliding friction coefficient and the load is shown in Fig. 4b. Based on this relationship, it can be concluded that the sliding friction coefficient of the silica gel increases with the increase of the load.

Figure 5 shows the results of the temporal changes in the friction force with different normal loads and the dynamic characteristics of the displacement fields of the silicone front side. Fig. 5a shows that the temporal changes in the friction force of the silicone with no additional normal load are similar to those for typical friction. During preliminary adjustment phase and deformation phase, the friction force is a static friction force. This friction force increased monotonically until it reached the critical point (maximum static friction). Then the silicone moved above the platform and the friction force decreased slightly until the end of the motion. The silicone moved smoothly without stick-slip for the entire motion. From 3.75 s to 6.75 s, it can be observed from the dynamic cloud diagram of the displacement field that a deformation wave was generated on the silicone surface with the same transmission direction as the direction of relative movement of the silicone to the module.

As shown in Table 1, the dynamic friction force when the silicone reaches steady-state motion has an obvious monotonically increasing relationship with the load. It is worth

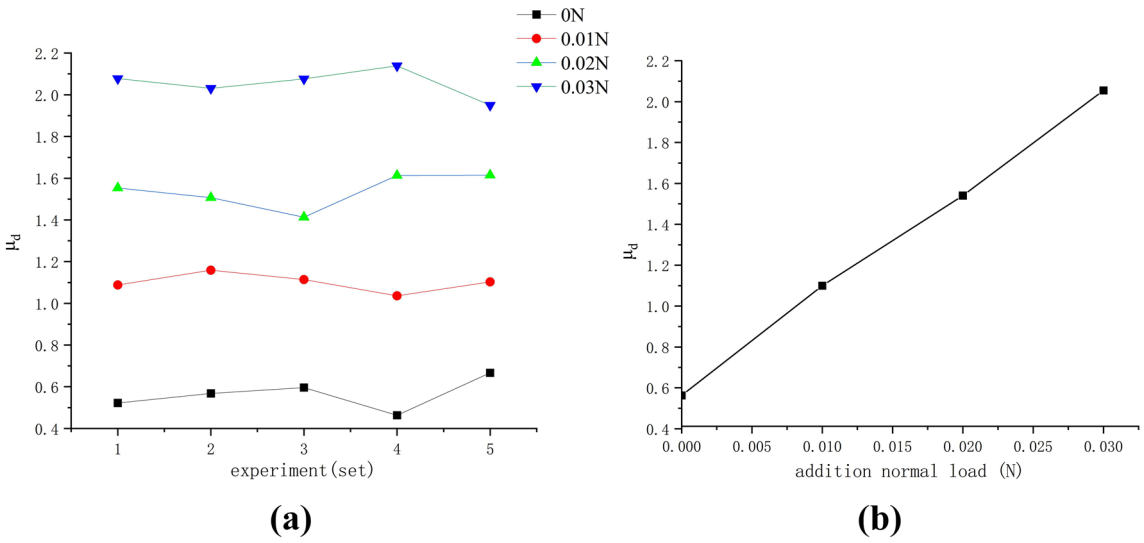

Fig. 4 Sliding friction coefficients of silicone under different normal loads, **a** five sets of data for each additional normal load; **b** value of sliding friction coefficient for each additional normal load

noting that the maximum static friction force was not very different from the dynamic friction force when there was no additional load. With the additional load, the maximum static friction was 2–3.5 times higher than the dynamic friction. Based on classical friction theory, the maximum static friction is slightly higher than the sliding friction. 2–3.5 higher maximum static friction than the dynamic friction for the sliding friction of silicone means that adhesive forces account for more than half of the composition of static friction. At the moment silicone broke free of adhesion from rest to movement, the stretching force of the connecting rope on the silicone was much greater than the sliding friction of the silicone, it caused a noticeable stick-slip phenomenon in the sliding friction silicone, and with the increase of the normal load, the stick-slip phenomenon was more significant.

Before the stick-slip occurred, a deformation wave was observed on the silicone surface from the right end to the left end. In particular, when the additional normal load was 0.03 N, the third deformation wave is transmitted from the middle of the silicone to the left end of the silicone. The transmission velocity of the first deformation wave did not differ very much for each normal load condition, but the transmission velocity of the second deformation wave was faster for the load increases.

The dynamic changes on both sides of the silicone (R0 region and R1 region) were most obvious during the motion, so these regions were chosen as the study area. The locations of the R0 region and the R1 region are shown in Fig. 6, The length of the R0 and R1 area is 10mm and the width is 6mm.

Figure 7 shows the displacement field variation curves at both sides of the silicone for four different normal loads. The displacement field distributions of R0 and R1 for all normal loads are symmetric about U = 0. The sliding friction of the silicone can be divided into the preliminary adjustment phase, deformation phase, stick-slip phase, steady-state motion phase, and relaxation phase.

(1) Preliminary adjustment phase: At this stage, the amount of silicone deformation fluctuates slightly at the zero point and is distributed irregularly. The strain field distribution on the side surface of the silicone is chaotically distributed, as shown in Fig. 8a. The reason for this phenomenon is that the silicone is a soft viscoelastic material and is not completely fitted to the surface when placed on the platform, and there are many gaps between the surfaces of the silicone and the platform. Therefore, the silicones make minor adjustments to deformation in the process of the relative movement trend until the surfaces are completely fitted.

(2) Deformation phase: At this stage, the displacement field curve grows at a high rate until it reaches a peak, and the strain field of silicone is symmetrically distributed at the center and remains stable, as shown in Fig. 8b. Macroscopic deformation is stretched from the center to both sides of the silicone, and deformation waves are generated at this stage.

(3) Stick-slip phase: At this stage, the displacement field curve reaches a peak and then drops to a trough at a very fast rate. Adhesion exists between the silicone and the platform surface. After the force reaches a critical point, the silicone breaks free from the adhesive force and jumps both vertically and in the direction of the connecting rope. In the process of jumping, the silicone resumes deformation from both sides to the center of

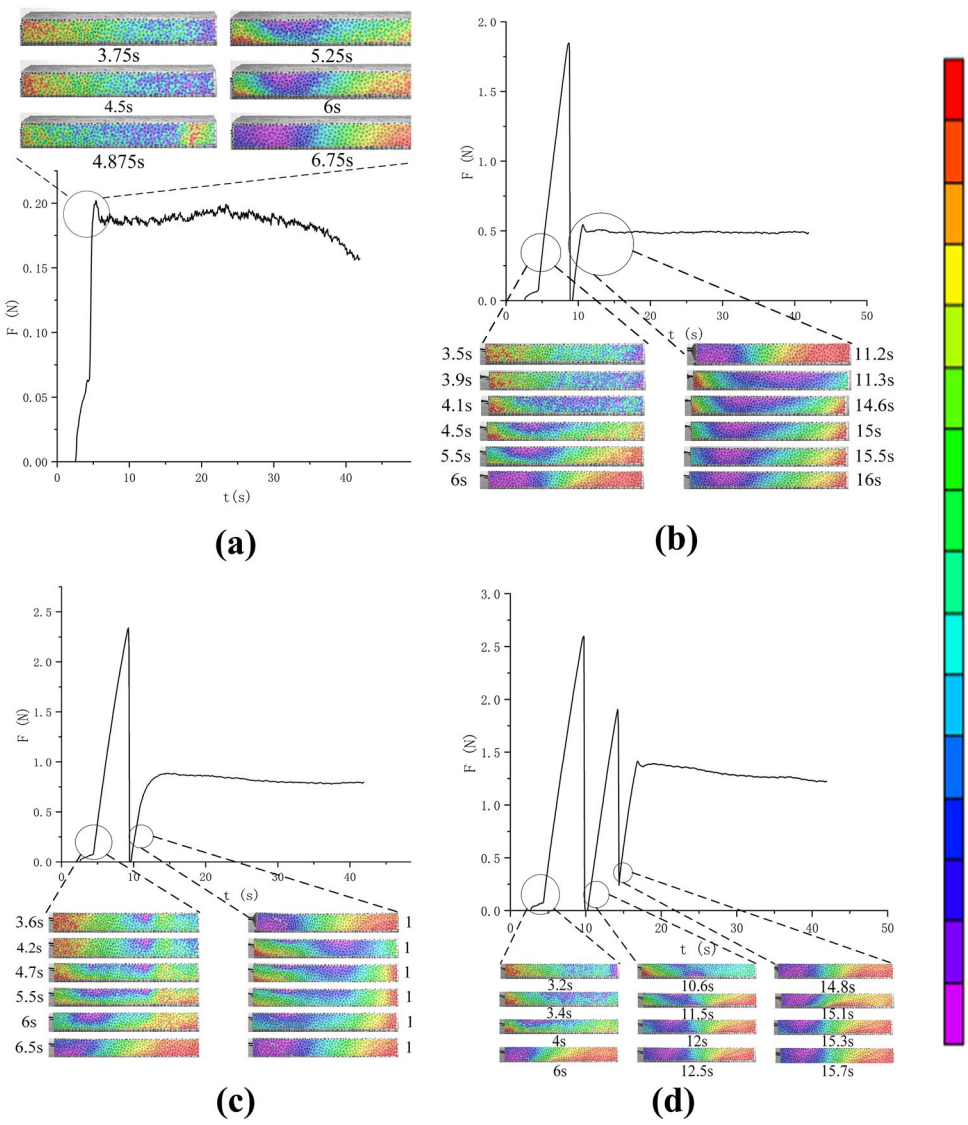

Fig. 5 Temporal changes in the friction force with different normal loads and the dynamic characteristics of the displacement fields of the silicone front side: **a** no additional normal load; **b** additional normal load is 0.01 N; **c** additional normal load is 0.02 N; **d** additional normal load is 0.03 N because the values of the colored contour plots are not the same at different moments because the values of the colored contour plots are not the same at different moments, a colored contour plot without values are added in Fig. 5 to indicate the amount of deformation, with purple indicating minimal deformation and red indicating maximum deformation (Color figure online)

Table 1 Data of sliding friction behavior under different load increments

Additional normal load (N)	Maximum static friction force (N)	Sliding friction force (N)	Duration of the first deformation wave (s)	Duration of the second deformation wave (s)	Duration of the third deformation wave (s)
0	0.202	0.17	3	–	–
0.01	1.848	0.49	2.5	5.8	–
0.02	2.158	0.73	2.9	2.5	–
0.03	2.595	1.27	2.8	1.9	0.9

the silicone until the bottom surface of the silicone is in contact with the platform surface again. The strain field distribution of the silicone is shown in Fig. 8c.

(4) Steady- state motion phase: At this stage, the displacement field curve remains in a relatively stable state, and the macroscopic deformation of the silicone does not change. The strain field of the silicone has a gradual distribution from left to right, as shown in Fig. 8d.

(5) Relaxation phase: At this stage, there is a small contraction at the end of the displacement field curve of the silicone, the strain field distribution is similar to that of the steady state motion phase, and the relative motion

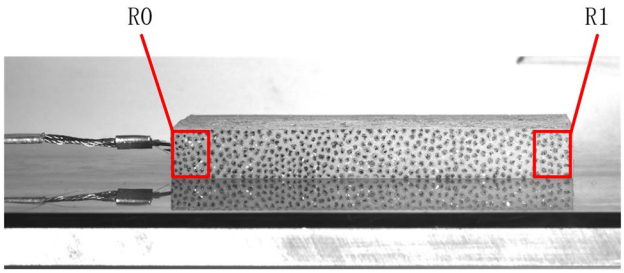

Fig. 6 Study area location

of the silicone and platform stops. Due to inertia, the silicone will continue to move before coming to rest. The static friction force at rest is less than the sliding friction force during steady motion, and the silicone macro deformation has small shrinkage and remains relaxed, as shown in Fig. 8e.

3.2 Dynamic Characteristics of the Silicone Tooth Structure Surface in Sliding Friction

The movement direction of the silicone tooth structure surface along the beveled edge of the tooth is the left-direction and along the right-angle edge of the tooth in the right-direction, as shown in Fig. 9.

Figure 10 shows five sets of sliding friction coefficient data for the silicone tooth structure surface moving along the left-direction and the right-direction. The average value of the sliding friction coefficient along the left-direction motion is 1.297 with a standard deviation of 0.084, and the average value of the sliding friction coefficient along the right-direction motion is 0.695 with a standard deviation of 0.106. It can be concluded that the sliding friction coefficient for the silicone tooth structure surface moving along the left-direction is greater than that for moving along the right-direction.

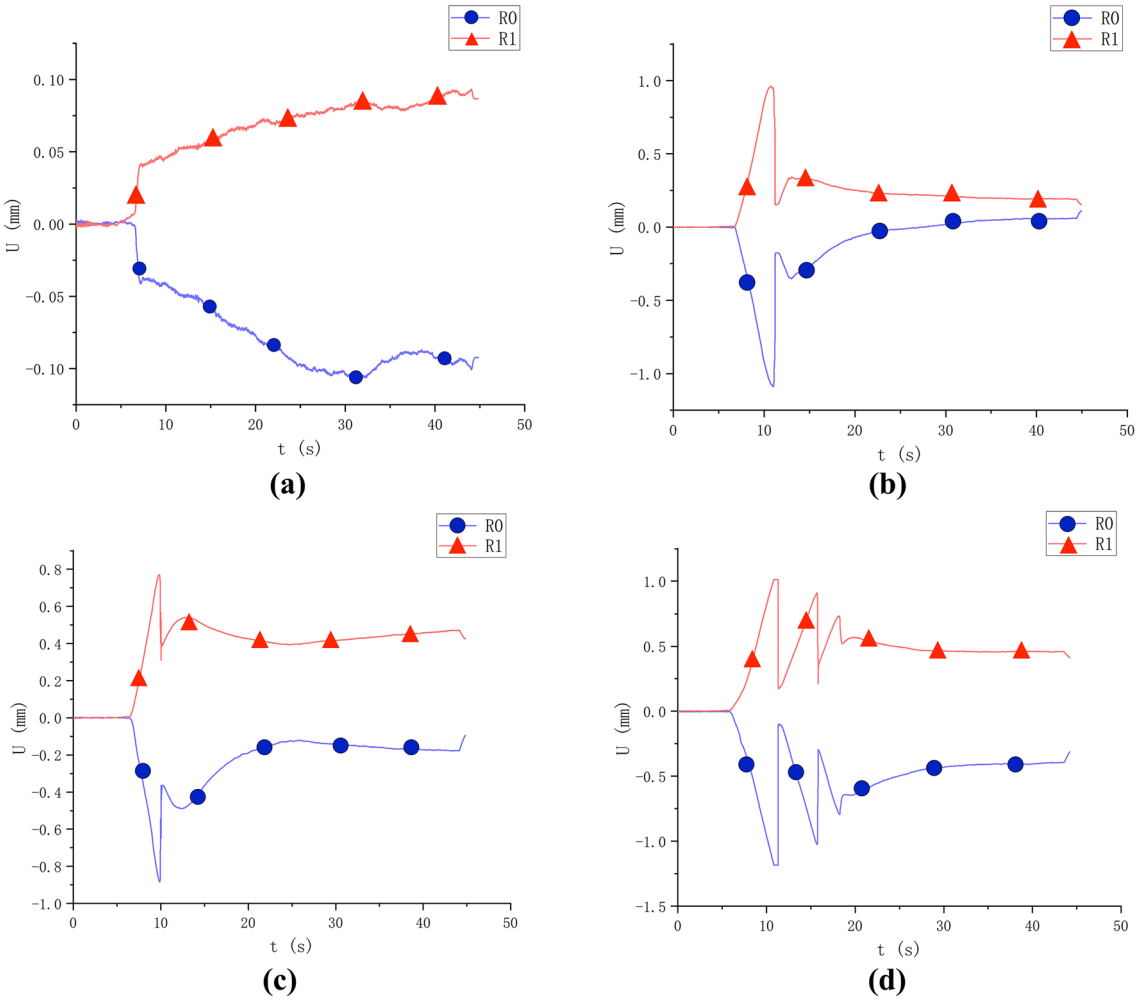

Fig. 7 Displacement field variation curves at both sides of the silicone for different normal loads, "U" is the average displacement of the speckles in study area: **a** no additional normal load; **b** additional normal load is 0.01 N; **c** additional normal load is 0.02 N; **d** additional normal load is 0.03 N

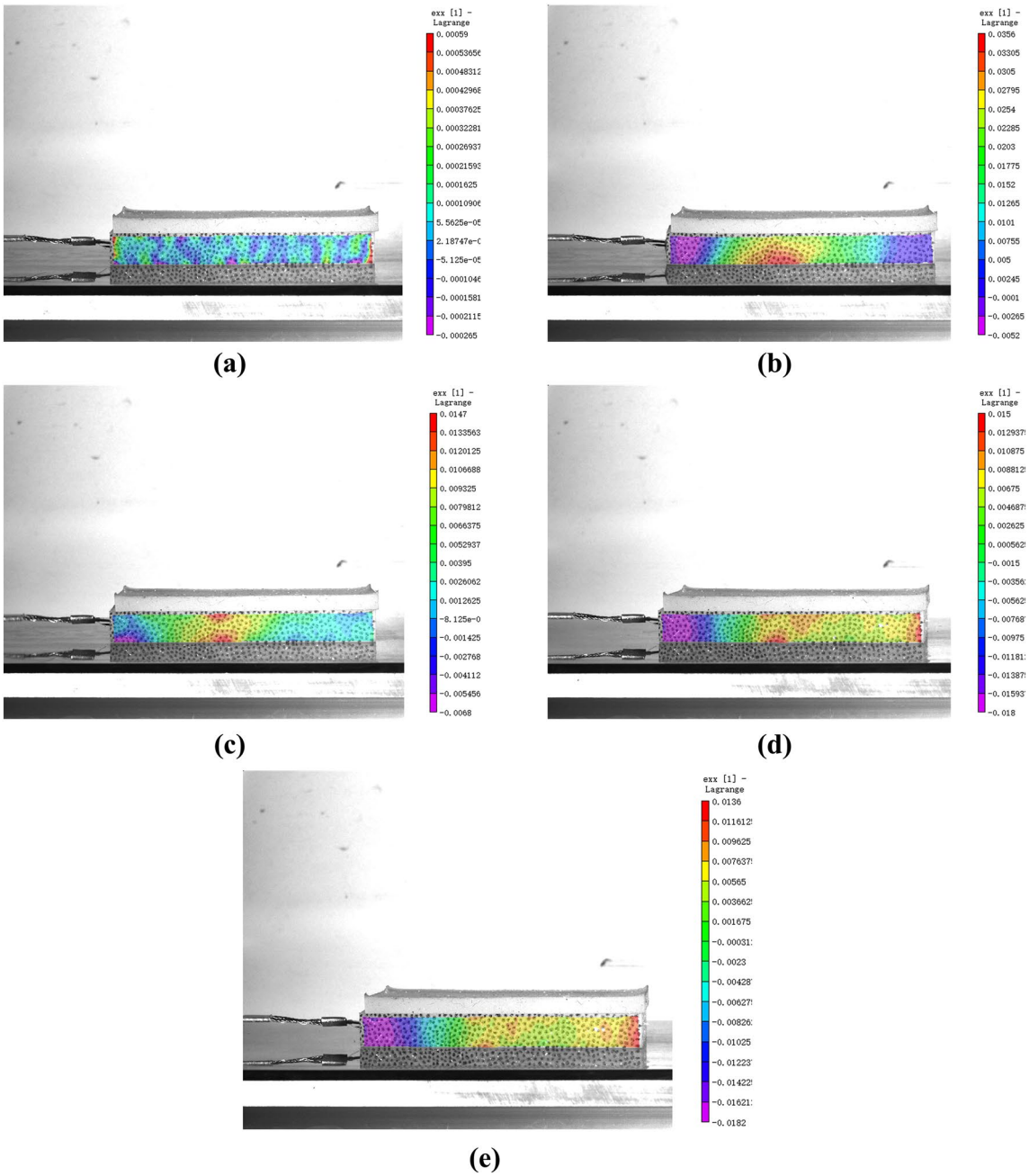

Fig. 8 Horizontal strain distribution at each stage of silicone sliding friction: **a** preliminary adjustment phase; **b** deformation phase; **c** stick-slip phase; **d** steady state motion phase; **e** relaxation phase

Figure 11 shows the results of the temporal changes in the friction force for different motion directions of the silicone tooth structure surface and the dynamic characteristics of the displacement field on the side surface of the silicone. For the case of a constant contact area and a normal load, the temporal changes in the friction force of the silicone tooth structure surface along the left-direction and the right-direction are similar to the state without an additional load described in Sect. 3.1. The silicone moves smoothly without stick-slip. The value of friction is greater along the left-direction than along the right-direction, and the time taken to reached the maximum static friction was slightly longer. In addition, during the motion along the right-direction, the deformation wave was transmitted from the right to the left in the same direction as the specimen motion at 2–2.75 s, and the deformation wave is not observed during the motion along the left-direction.

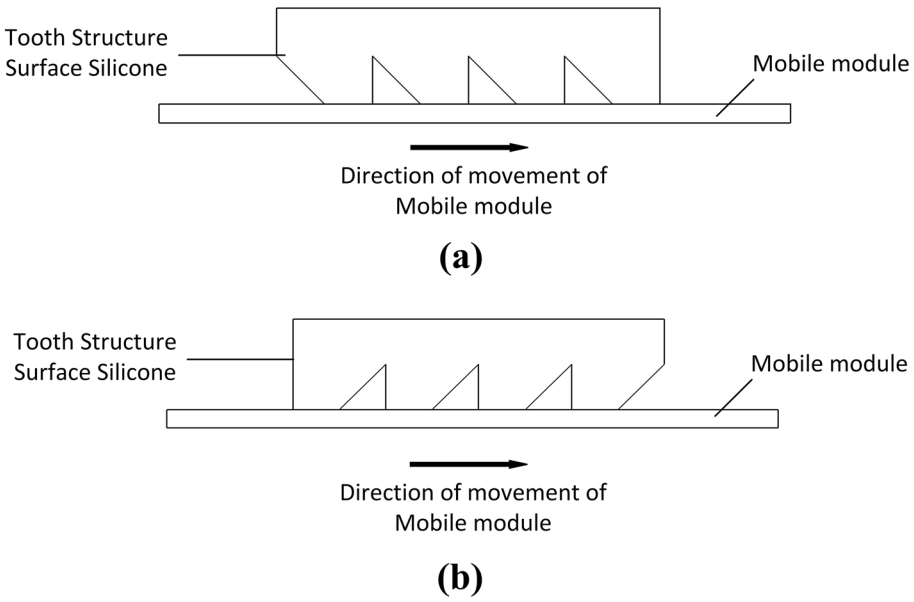

Fig. 9 Tooth structure surface silicone movement direction: **a** Left-direction; **b** Rigth-direction

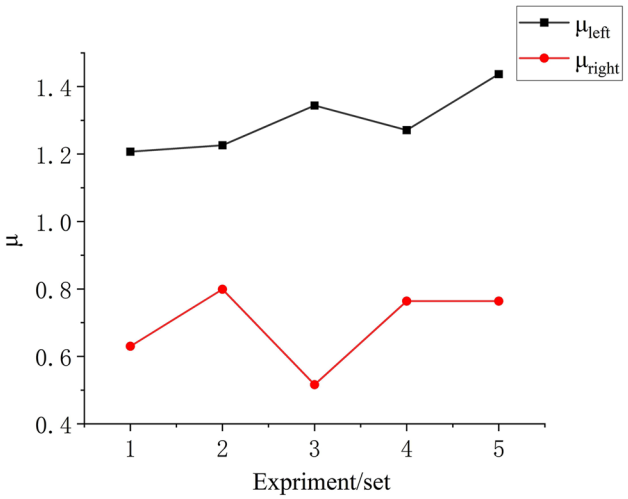

Fig. 10 Friction force data of tooth structure surface silicone in different movement direction

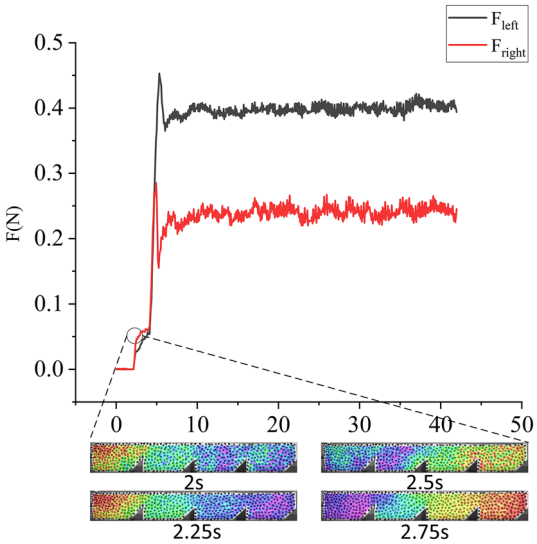

Fig. 11 Dynamic characteristics of sliding friction and displacement field clouds of tooth structure surface silicone in different movement direction, and the displacement fields are for z-direction

The displacement field cloud diagram of the silicone tooth structure surface in motion along the left-direction is shown in Fig. 12a. The displacement field is asymptotically distributed that the displacement field clouds are stratified from right to left and the values are increasing, the zero position is in the center of the silicone. The macroscopic deformation of the silicone is in a stretched state, resulting in a larger actual contact area between the silicone and the platform. When moving along the right-direction, the displacement field distribution is symmetrical about the center, and the macroscopic deformation of silicone is in a flexural state, as shown in Fig. 12b, resulting in a reduction of the actual contact area between the silicone and the platform.

The silicone tooth structure surface moving along the left-direction is greater than that moving along the right-direction. The reason for this phenomenon is that the deformation of the specimen during the motion results in the actual contact area being different.

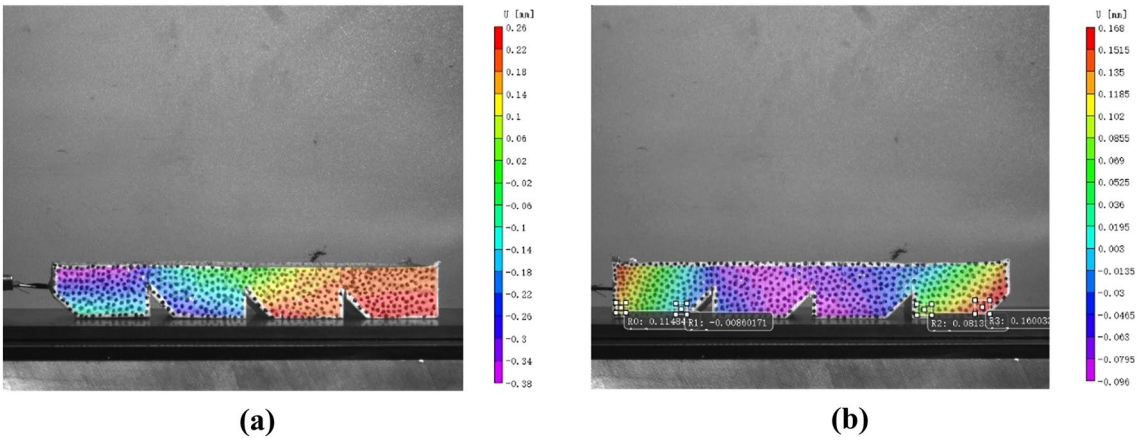

Fig. 12 Displacement field clouds of tooth structure surface silicone specimens with different motion directions in steady movement state: **a** left-direction; **b** right-direction

4 Discussion

According to the sliding friction analysis of silicone discussed in the previous section, it is concluded that the sliding friction coefficient has the same increasing relationship with the normal load, and there are macroscopic friction behaviors such as deformation wave and stick-slip during the sliding friction process. In this section, the macroscopic friction behavior of the silicone and the reason for the variation of the sliding friction coefficient with the load are discussed.

4.1 Macroscopic Sliding Friction Behaviors of Silicone

Barquins [10, 18–20] published a series of experimental studies on the friction behaviors of rubber-like materials on rigid surfaces, and described the measurement process in three phases according to the status of the contact surface: preliminary (pre-sliding) phase, gross sliding phase, and relaxation phase. Based on his research, in this study, the preliminary phase is further subdivided into the preliminary adjustment phase and the deformation phase, and the gross sliding phase is further subdivided into the stick-slip phase and the steady state motion phase. The distribution of strain on the surface of silicone undergoes three types of changes: irregular, symmetrical and asymptotical. During the steady-state motion phase, the local area close to the connection point of silicone to rope is the flexural area, and the local area far from connection point of silicone to rope is the tensile area.

The stick-slip effect for the sliding friction of the soft viscoelastic materials can be treated as a repetition of the following phases [21]:

(1) Sticking to the surface while the deformation and the friction force keep growing.
(2) Breaking away when the break-away force is reached and the friction state switches from static to kinetic or from sticking to sliding.
(3) Back to sticking to the surface. The deformed rubber material retracts and even overshoots after breaking away. Its relative velocity relative to the contact surface decreases to zero and it sticks to the surface again.

In the experiments of this study, it is observed that the stick-slip effect of silicone is more significant with the increase of the load in a certain load range, which can be judged using the wider macroscopic deformation of silica gel, greater separation force, and greater number of occurrences. In addition, the stick-slip phenomenon of the jump amplitude gradually decreases for a certain normal load sliding friction. The reason for this is that the magnitude of the break-away force is related not only to the load but also to the length of contact time between two surfaces and the height of the jumping after the stick-slip. The higher the height of the silicone vertical jump is, the greater the normal force after recontact is, resulting in greater adhesive force. Therefore, the stick-slip phenomenon is gradually decreasing for a certain normal load. It can be expected that stick-slip will fill the whole sliding friction process when the load continues to increase.

The reason for the generation of deformation waves is that the tensile force is gradually transmitted from the left to the right of the silicone. The deformation waves show the process of the silicone from the static state to the relative motion trend state. Therefore, deformation waves mainly occur during the transition from the preliminary adjustment phase to the deformation phase and the transition from static to motion states after the stick-slip.

Because the normal load has very little effect on the preliminary adjustment phase, the first deformation wave is transmitted at the same speed. In addition, the increase in the normal load leads to greater deformation of the silicone and less recovery of deformation after stick-slip. Therefore, the deformation wave in the stick-slip phase is transmitted faster with the increases in the normal load.

At present, many scholars are currently more interested in the Schallamac wave phenomenon generated during the motion between rubber-like materials and rigid materials [9]. A Schallamac wave is formed when hemispherical transparent glass slides on rubber. The rubber and the glass adhere to form a cavity, and the cavity moves along the curved surface of the glass. In this study, the focus is on the sliding friction between silicone and metal, and it is not deemed appropriate to observe the state of the silica gel contact surface, so the Schallamac wave is not observed. The deformation waves observed in this study occur on the side of the silicone. This is also due to the deformation of the silicone and perhaps has some correlation with the s-wave. However, the deformation wave observed in this study, which occurs on the side of the silicone, is also due to silicone deformation and perhaps has some correlation with the Schallamac wave. The method proposed in this paper for the measurement of the dynamic friction force and the deformation-strain optical non-contact measurement based on DIC may have some applicability in the study of Schallamac waves.

4.2 Reasons for Monotonically Increase of Sliding Friction Coefficient with Load

The surfaces of the objects are not ideal planes and there are irregular bumps. Hence, in the two objects, the contact plane is not completely in contact. According to Hertz's contact law[22–24], the surface of the object is assumed to be composed of a uniform distribution of hemispherical raised peaks , as shown in Fig. 13a. A_0 is the theoretical contact area, it means the cross-sectional area of the contact surface, A_c is the actual contact area, it indicates the contact area between the surface covered with much raised peaks. μ_0 is the theoretical friction coefficient based on the theoretical contact area. μ_c is the actually friction coefficient based on the actually contact area.

$$\mu_c = \mu_0 A_c / A_0 \tag{1}$$

Figure 13b indicated the cut of contact surface between the surface covered with much raised peaks, When two raised peaks come into contact, deformation occurs due to compression. R_c is the radius of the actual contact surface. The radius of the raised peak of the platform is R_1 and the radius of the raised peak of the silicone is R_2.

$$R_c = 2R_1R_2/(R_1 - R_2) \tag{2}$$

Because silicone is a soft viscoelastic material and the platform is a rigid metal material, the deformation of the

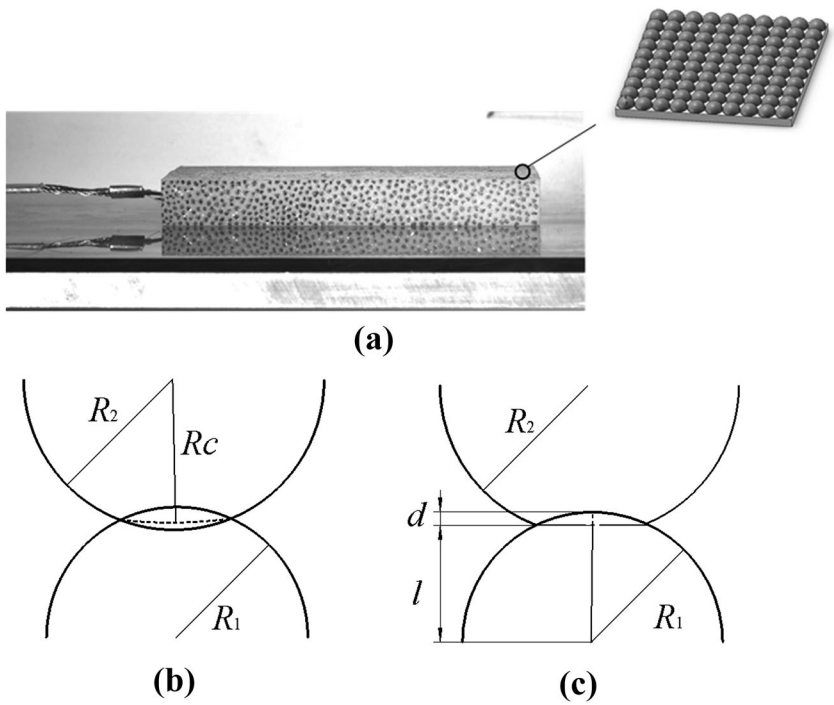

Fig. 13 Hertz elastic contact: **a** surface of silicone; **b** contact to theoretical conditions; **c** contact between soft viscoelastic material and rigid material

raised peaks on the metal surface when in contact is much smaller than the deformation of the raised peaks on the silicone surface. Therefore, it is considered that the platform surface does not deform and the deformation is only produced by the silicone surface, as shown in Fig. 13c.

$$R_c = R_2 \tag{3}$$

The CMT6503 Universal Material Testing Machine was used for this experiment, as shown in Fig. 14a. The displacement at the compression end was used as the specimen deformation variable and the force applied to the specimen by the force transducer was recorded. The data were collected and entered into the computer to obtain a graph of the force versus the amount of silicone deformation, as shown in Fig. 14b.

The relationship between the macroscopic deformation and the load is shown as follows:

$$d = 9.38 - 5.8e^{-F_z/34.48} - 3.67e^{-F_z/229.05} \tag{4}$$

The actual contact area A_c:

$$A_c = 2n\pi \int_{R_c-l}^{R_c} \sqrt{R_c^2 - x^2}\sqrt{\frac{R_c^2}{(R_c^2 - x^2}}dx = 2n\pi R_c(R_c - d) \tag{5}$$

In equation 5, n indicates the number of raised peaks.

Combining Eqs. (4) and (5):

$$A_c = 2n\pi R_c(R_c + 5.8e^{-F/34.48} + 3.67e^{-F/229.05} - 9.38) \tag{6}$$

The equation for the actual contact area and the load that is derived in this research is similar to that of the study in [25].

The nominal contact area A_0:

$$A_0 = 4nR_c^2 \tag{7}$$

Combining Eqs. (1), (6), and (7), the relationship between the sliding friction coefficient and the load is shown as follows:

$$\mu_c = 2\pi\mu_0(R_c + 5.8e^{-F/34.48} + 3.67e^{-F/229.05} - 9.38)/R_c \tag{8}$$

From Eq. (8), it can be concluded that the sliding friction coefficient increases with the increase of the load. Compared to the monotonically increasing relationship between the normal load and sliding friction coefficient derived from the theoretical model, in the experiments of this research, only the sliding friction coefficient under four different loads is investigated. It is possible to prove that the sliding friction coefficient has the same increasing relationship with the load, but the sample size is small enough to completely prove the detailed mathematical relationship between the normal load and the sliding friction coefficient. In addition, the load affects not only the actual contact area but also the adhesion in a non-drying condition [26].

5 Conclusion

In this study, a research method combining a dynamic force testing technique and a non-contact optical testing technique for deformation and strain was used to determine the sliding friction of silicone. The temporal changes in the friction force in different loads and the dynamic characteristics of the deformation and strain on the side surface of the silicone were obtained, and the following conclusions were drawn.

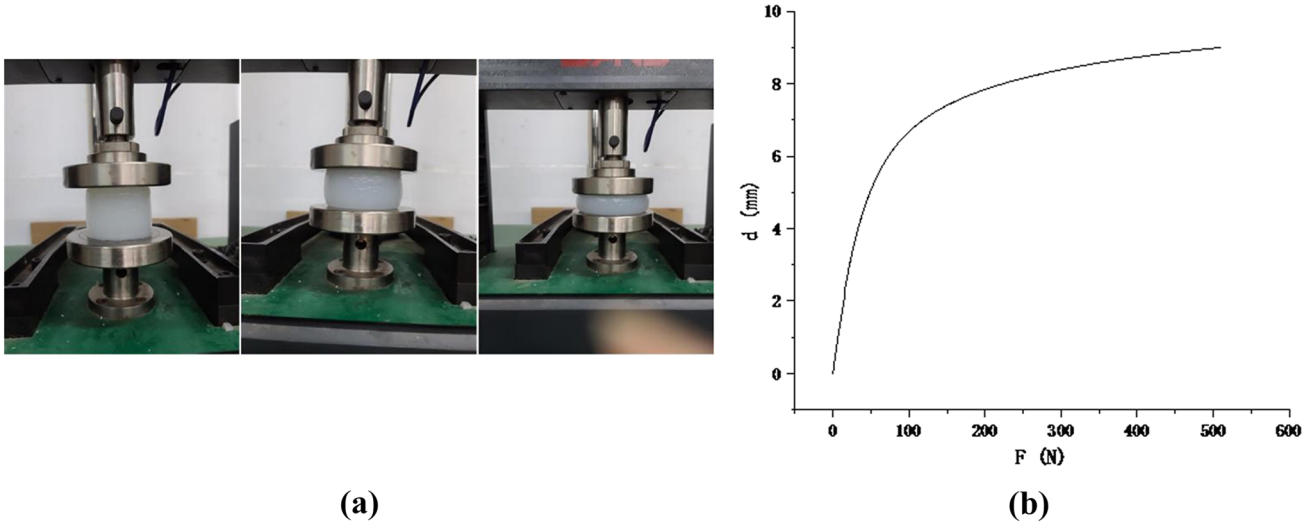

Fig. 14 Relationship between silicone deformation and normal load: **a** measurement method **b** curve

(1) The sliding friction of silicone can be divided into the preliminary adjustment phase, deformation phase, stick-slip phase, steady state motion phase, and relaxation phase.
(2) The macroscopic frictional behavior of silicone includes the deformation waves, stick-slip, and dynamic processes of silicone deformation.
(3) Deformation waves mainly occur during the transition from the preliminary adjustment phase to the deformation phase and during the transition from a static state to motion after stick-slip. The transmitted direction is the same as the direction of movement, and the deformation wave caused by the stick-slip accelerates the transmission speed with the increase of the load.
(4) The larger the normal load of the silicone is, the more significant the stick-slip phenomenon is, and the amplitude of the stick-slip is gradually smaller for a certain normal load.
(5) In a certain load range, the sliding friction coefficient of the silicone has the same increasing relationship with the load.
(6) The shape of the silicone has a significant effect on the coefficient of sliding friction. For example, the tooth structure silicone is characterized by the anterior-posterior anisotropy of the sliding friction.

Acknowledgements I would like to thank my advisors and lab mates for helping with the experiments.

Author Contributions All authors contributed to the study conception and design. Material preparation, data collection and analysis were performed by YG,YW: directed the experimental design and writing, and all authors commented on previous versions of the manuscript. All authors read and approved the final manuscript.

Funding Information The authors declare that no funds, grants, or other support were received during the preparation of this manuscript.

Declarations

Conflict of Interest The authors have no relevant financial or non-financial interests to disclose.

References

1. Wright, C., Johnson, A., Peck, A., Mccord, Z., Choset, H.: Design of a modular snake robot. In: Intelligent robots and systems, 2007. IROS 2007. IEEE/RSJ International Conference on (2007)
2. Ouyang, W., Liang, W., Li, C., Zheng, H., Ren, Q., Li, P.: Steering motion control of a snake robot via a biomimetic approach. Front. Info. Technol. Electron. Eng. **20**(1), 32–44 (2019)
3. Bangar, M.G., Nirgude, H.S., Ghodake, S.P., Ohol, S.S.: Autonomous snake robot with serpentine type navigation. IOP Conf. Ser. Mater. Sci. Eng. **1012**, 012027 (2021)
4. Tanaka, M., SawaBe, H., Nakajima, M., Ariizumi, R.: Redundant control of a planar snake robot with prismatic joints. Int. J. Control Auto. Syst. **19**, 3475–3486 (2021). https://doi.org/10.1007/s12555-020-0607-2
5. Meng, L., Sheng, W., Wang, Y.: Analysis and simulation of motion characteristics of silkworm-robot. Mech. Sci. Technol. Aerospace Eng. **20**(1), 443–457 (2018). https://doi.org/10.13433/j.cnki.1003-8728.20180025
6. Kamamichi, N.: Design and implementation of a lizard-inspired robot. Appl. Sci. **11**(17), 7898 (2021). https://doi.org/10.3390/app11177898
7. Schallamach, A.: How does rubber slide? Wear **17**(4), 301–312 (1971)
8. Maegawa, S., Nakano, K.: Dynamic behaviors of contact surfaces in the sliding friction of a soft material. J. Adv. Mech. Des. Syst. Manuf. **1**(4), 553–561 (2007)
9. Wu, Y., Varenberg, M., Leamy, M.J.: Schallamach wave-induced instabilities in a belt-drive system. J. Appl. Mech. **86**(3), 031002 (2018)
10. Barquins, M.: Sliding friction of rubber and schallamach waves—a review. Mater. Sci. Eng. **73**, 45–63 (1985). https://doi.org/10.1016/0025-5416(85)90295-2
11. Ringoot, E., Roch, T., Molinari, J.-F., Massart, T.J., Cohen, T.: Stick-slip phenomena and schallamach waves captured using reversible cohesive elements. J. Mech. Phys. Solids **155**, 104528 (2021)
12. Maegawa, S., Nakano, K.: Mechanism of stick-slip associated with schallamach waves. Wear **268**(7–8), 924–930 (2010)
13. Tiwari, A., Tolpekina, T., Benthem, H.V., Gunnewiek, M.K., Persson, B.: Rubber adhesion and friction: role of surface energy and contamination films. Front. Mech. Eng. (2021). https://doi.org/10.3389/fmech.2020.620233
14. Prevost, A., Scheibert, J., Debrégeas, G.: Probing the micromechanics of a multi-contact interface at the onset of frictional sliding. Euro. Phys. J. E **36**(2), 17 (2013)
15. Satoru, M., Fumihiro, I., Takashi, N.: Dynamics in sliding friction of soft adhesive elastomer: schallamach waves as a stress-relaxation mechanism. Tribol. Int. **96**, 23–30 (2016). https://doi.org/10.1016/j.triboint.2015.11.034
16. Kirugulige, M.S., Tippur, H.V., Denney, T.S.: Measurement of transient deformations using digital image correlation method and high-speed photography: application to dynamic fracture. Appl. Opt. **46**(22), 5083–5096 (2007)
17. Tuononen, A.J.: Digital image correlation to analyse stick-slip behaviour of tyre tread block. Tribol. Int. **69**, 70–76 (2014)
18. Barquins, M.: Friction and wear of rubber-like materials. Wear **160**(1), 1–11 (1993)
19. Barquins, M., Courtel, R.: Rubber friction and the rheology of viscoelastic contact. Wear **32**(2), 133–150 (1975)
20. Barquins, M., Roberts, A.D.: Rubber friction variation with rate and temperature: some new observations. J. Phys. D: Appl. Phys. **19**, 547 (1986). https://doi.org/10.1088/0022-3727/19/4/010
21. Rs, A., Mw, B., Mz, A.: A model for the dynamic friction behaviour of rubber-like materials. Tribol. Int. **164**, 107220 (2021). https://doi.org/10.1016/j.triboint.2021.107220
22. Guanghui, Fu.: An extension of hertz's theory in contact mechanics. J. Appl. Mech. **74**(2), 373–374 (2006)
23. Yan, W., Fischer, F.D.: Applicability of the hertz contact theory to rail-wheel contact problems. Archive of Applied Mechanics. **70**, 255–268 (2000). https://doi.org/10.1007/s004199900035

24. Machado, M., Moreira, P., Flores, P., Lankarani, H.M.: Compliant contact force models in multibody dynamics. Evolution of the hertz contact theory. Mech. Mach. Theory **53**, 99–121 (2012)
25. Hemette, S., Cayer-Barrioz, J., Mazuyer, D.: Thermal effects versus viscoelasticity in ice-rubber friction mechanisms. Tribol. Int. **162**(3), 107129 (2021)
26. Deleau, F., Mazuyer, D., Koenen, A.: Sliding friction at elastomer/glass contact: Influence of the wetting conditions and instability analysis. Tribol. Int. **42**(1), 149–159 (2009)